Emulation of Multi-Inverter Integrated Weak Grid via Interaction-Preserved Aggregation

Liao, Shuhan; Huang, Meng; Zha, Xiaoming; Guerrero, Josep M.

Published in:
IEEE Journal of Emerging and Selected Topics in Power Electronics

DOI (link to publication from Publisher):
10.1109/JESTPE.2020.2988364

Publication date:
2021

Document Version
Accepted author manuscript, peer reviewed version

Emulation of Multi-Inverter Integrated Weak Grid via Interaction-Preserved Aggregation

Shuhan Liao, *Student Member, IEEE*, Meng Huang, *Member, IEEE*, Xiaoming Zha, *Member, IEEE*, Josep M. Guerrero, *Fellow, IEEE*

***Abstract*— Simplified weak grid models are widely used to emulate the non-ideal power grid for the design and stability analysis of grid-connected inverters. However, the dynamic behavior of a real grid with multiple inverters is complex. In this paper, an emulation method is proposed for multi-inverter integrated weak grids using an interaction-preserved aggregation model associated with grid impedance. Firstly, the interaction among inverters in weak grids is analyzed using the state-space model and participation analysis. Then, two-inverter aggregation is proposed for a large-scale system. This model can preserve the impact of parameters on the interaction modes (IMs), and predict the IM-related instability of multi-inverter systems. Thus, the two-inverter representation is applied to emulation to preserve interactions and to simplify the testing of multiple inverters. The emulation of the 16-inverter system is implemented on a hardware-in-the-loop (HIL) test bench with one practical inverter controller under test and remaining parts integrated in the OPAL-RT real-time simulator. The test results show that the instability attributed to interaction can be identified by the proposed emulation method.**

***Index Terms*— Grid Emulation, multiple inverters, aggregation modeling, interaction, grid-connected microgrids.**

NOMENCLATURE

S	Capacity of an inverter.
L_f	Filter inductance of an inverter.
C	DC-link Capacitance.
L_g	Equivalent inductance of a weak grid.
R_g	Equivalent resistance of a weak grid.
v_g	Infinite bus voltage.
i_{abc}	Line currents of an inverter in the three-phase stationary frame.
I_{dq}	*D*-axis and *q*-axis current components of currents
U_{dc}	DC-link voltage of an inverter.
$u_{abc,ref}$	Modulating voltage for three-phase modulation.
U_{dqref}	Modulating voltage in the *dq* rotating reference frame.
v_p	Voltage at the point of common coupling (PCC).
θ_{pll}	The phase output of PLLs.
ω_{pll}	The frequency output of PLLs.
θ_g	Phase of grid voltage.
θ	Difference between θ_{pll} and θ_g.
ω	Derivative of θ.
γ	The derivative of i.
g	Gate driving signals.
k_{pv}, k_{iv}	Proportional and integral coefficients of dc voltage loop.
k_{pi}, k_{ii}	Proportional and integral coefficients of current control loop.
k_{pt}, k_{it}	Proportional and Integral coefficients of PLL.
P_{in}	Power input from constant power sources.
I_g	Grid current.

Subscripts

a, *b*, *c*	Components in the three-phase stationary frame.
x, *y*	*X*-axis and *y*-axis components in the *xy* rotating reference frame.
d, *q*	*D*-axis and *q*-axis components in the *dq* rotating reference frame.
ref	The reference value.
0	Initial value.
j=1, 2, 3…	The serial number of inverters.
k=1, 2, 3…	The serial number of state variables.
l=1, 2, 3…	The serial number of modes.
eq	Equivalent parameters of aggregated models.

Manuscript received December 1, 2019; revised January 29, 2020 and March 24, 2020; accepted April 10, 2020. This work was supported by the National Natural Science Foundation of China (51637007, 51877159, U1866601). (*Corresponding author: Meng Huang*)

Shuhan Liao, Meng Huang, and Xiaoming Zha are with School of Electrical Engineering and Automation, Wuhan University, Wuhan, China (e-mail: shuhanliao@whu.edu.cn; meng.huang@whu.edu.cn; xmzha@whu.edu.cn).

Josep M. Guerrero is with the Department of Energy Technology, Aalborg University, 9220 Aalborg, Denmark (joz@et.aau.dk). J.M. Guerrero was funded by a Villum Investigator grant (no. 999730) from The Villum Foundation.

I. INTRODUCTION

A NUMBER of inverters in parallel is widely used in modern power systems to meet the increasing demand of large-scale renewable energy generation (RPG) in applications such as photovoltaic systems, wind farms or microgrids [1]. Because inverters are significant interface for RPG, the stable operation of multi-inverter systems is critical for the security and reliability of RPG-integrated power systems.

Testing on multi-inverter systems is an important step for parameter design and stability analysis. Grid impedance together with an ideal voltage source is used to emulate weak grid for inverters testing [2-4]. For the parameter design of a renewable power plant with multiple inverters, testing the same number of inverters with this grid emulator is complex and costly, even though the rating of tested inverters can be down

This article has been accepted for publication in a future issue of this journal, but has not been fully edited. Content may change prior to final publication. Citation information: DOI 10.1109/JESTPE.2020.2988364, IEEE Journal of Emerging and Selected Topics in Power Electronics

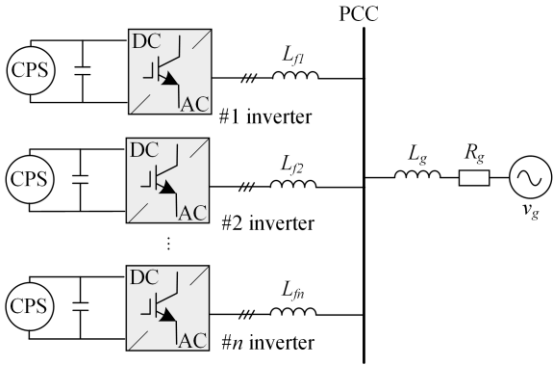

Fig. 1. The diagram of multiple paralleled inverters.

scaled by rescaling the parameters [5]. Thus, a simplified representation of multiple weak-grid-tied inverters is indispensable for emulation and testing.

Aggregation is a structure-preservation equivalence method to represent the dynamic characteristics of large-scale paralleled inverters in a simplified way [6-11]. In this method, the multiple identical or coherent inverters [9-11] are aggregated as a single up-scaled inverter, which has the same structure with actual inverters. The single-inverter aggregated model can preserve the external characteristics of multiple inverters, so it is effective for the analyses that focus on the stability of the system outside the inverters [8], [12]. However, this single-inverter aggregation method cannot reveal the interactions among inverters, and thus it is inadequate for the stability of a cluster of inverters itself.

In addition to aggregating inverters as an up-scaled one, another single-inverter representation method, which has the same capacity as that of each inverter in the actual system, is proposed in [13], [14]. This single-inverter representation is developed based on the phenomenon of multiplication effect reported in [13], which refers to that each inverter perceives N times impedance than that in the actual system. The single-inverter representation proposed in [13], [14] is intrinsically the same with the aggregated inverter with capacity multiplied. It is also reported in [13] that only the external stability of the equivalent inverter proposed in this paper coincide with that of the actual system.

In weak grids, the stability of paralleled inverters is different from that of a single inverter, due to the current interactions among inverters [13-18]. Linearized state-space modeling of inverters is one of the effective ways to investigate inverter interactions [19-22]. The component connection method (CCM) is a computationally efficient way to formulate the state-space model of a system composed of multiple inverters [20-22]. This approach partitions a system into individual components, and assembles the component models together as the composite state-space model. The participation analysis can be conducted on the state-space model to identify interaction modes and to specify which inverters or which state variables dominantly contribute to interaction modes [19]. However, when a large number of inverters are connected to the grid, the order of the state-space model established by CCM is still high. In addition, the stability problems arising from interaction among inverters have also been analyzed by multi-input multi-output (MIMO) impedance-based models in [13-18]. It has been concluded in [13], [14] that only when both external and internal poles are on the left-half plane, a cluster of paralleled inverters is stable. Similar to [13] and [14], the stability criterion of paralleled inverters concluded in [15], [16] is that they are both commonly and interactively stable. Therefore, even though the parameters are well designed for a single inverter, paralleled inverters may still suffer from stability problems attributing to interactions among them. In this way, the testing of a multi-inverter system should be conducted considering the impact of interactions. The MIMO impedance modeling of paralleled inverters is effective and efficient for identification of instability resulting from interactions, but it cannot be used for hardware test of paralleled inverters.

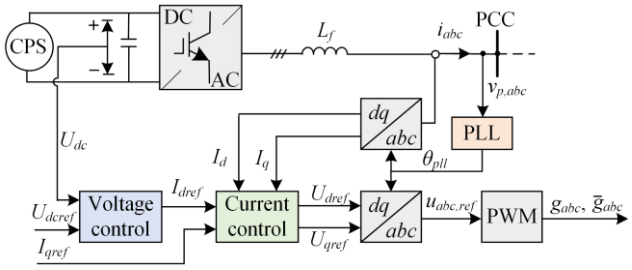

Fig. 2. The control diagram of a VOC-controlled grid-connected inverter.

TABLE I
PARAMETERS OF EVERY INVERTER

Symbols	S (MW)	L_f (mH)	C (10^3μF)	k_{pv}	k_{iv}	k_{pi}	k_{ii}	k_{pt}	k_{it}
Values	1.5	0.2	11.75	3	20	0.024	20	50	900

In this paper, an emulation method of multi-inverter integrated weak grids is proposed based on two-inverter aggregation, in order to preserve the interaction characteristics and to simplify the testbed simultaneously. Grid-connected inverters in renewable energy generation applications, like wind and solar power generation, are of concern in this paper. Because the dynamic response of inverters is faster than the change of wind speed and irradiance, the power input in the dc side of inverters is considered as constant [9]. The circuit configuration of multiple L-filter inverters is shown in Fig. 1, in which CPS is the abbreviation of constant power source. The inverters are controlled by voltage orientation control (VOC). The control diagram is shown in Fig. 2, where voltage controller and current controller are both PI controller and the phase-locked loop is a conventional synchronous reference frame PLL (SRF-PLL) [23].

The rest of the paper is organized as follows. In section II, interaction phenomena among paralleled identical inverters are presented, and the concepts of controllability and observability are used to extract the interaction characteristics. On this basis, the two-inverter aggregation representation is developed in section III to preserve the interactions, and a novel emulation method for multi-inverter integrated weak grid is presented using this aggregation. In section IV, the proposed aggregation method is verified by simulation of the example system with 16 inverters connected. A controller hardware-in-loop (HIL) test bench is also built in section IV to analyze the stability of the example system. Finally, Section V concludes the paper.

This article has been accepted for publication in a future issue of this journal, but has not been fully edited. Content may change prior to final publication. Citation information: DOI 10.1109/JESTPE.2020.2988364, IEEE Journal of Emerging and Selected Topics in Power Electronics

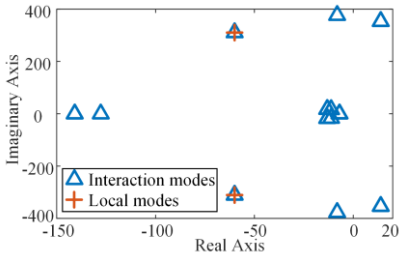

Fig. 3. Modes of three paralleled inverters connected to the weak grid (SCR=3).

TABLE II
IMS AND CORRESPONDING OPI

SN of modes	Eigenvalues λ	Damping ratio ξ	Frequency f (Hz)	OPI η
1, 2	-8.14±j376.72	2.16%	59.97	η_{11}=33.3% η_{21}=33.3% η_{31}=33.3%
3, 4	13.91±j353.45	-3.93%	56.30	**η_{12}=66.6%** **η_{22}=13.5%** **η_{32}=19.9%**
6, 7	13.91±j353.45	-3.93%	56.30	**η_{13}=0.00** **η_{23}=53.2%** **η_{33}=46.8%**

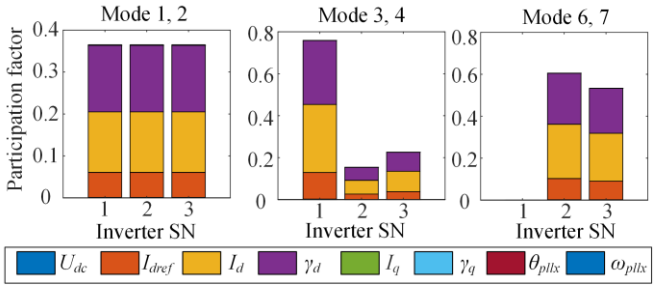

Fig. 4. Participation factors of medium-frequency IMs.

II. INTERACTION PHENOMENA AND CHARACTERISTICS

In this section, a system with three identical inverters connected to a weak grid (SCR=3) is taken as an example to explore the interaction phenomena and characteristics. The parameters of each inverter are listed in Table I and the phase-to-phase grid voltage v_g is 690V. The reference of q-axis current is 0 for three inverters. The meanings of symbols in Table I have been listed in the nomenclature. The parameters of the current loop, voltage loop, and the PLL are designed independently based on the open-loop transfer function of each loop. The bandwidths of the current loop, voltage loop, and the PLL are 447 rad/s, 51.5 rad/s, and 31.8 rad/s, respectively, and the phase margin of three loops ensures the stability of the three loops.

The interactions among inverters are identified based on the concept of participation factor. When the state variables of at least two inverters participate in the same mode, interactions exist and this mode is defined as an interaction mode (IM) [19]. To quantify the interaction among inverters, an overall participation index (OPI) for inverter j in mode l is defined [19]

$$\eta_{jl} = \frac{\left|\mathbf{p_{j,l}}\right|_1}{\left|\mathbf{p_l}\right|_1} \quad , \tag{1}$$

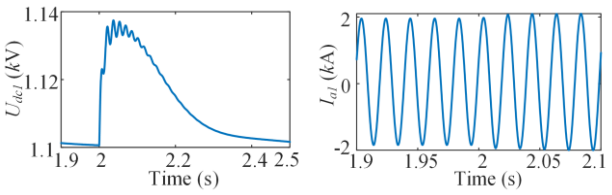

(a) (b)

Fig. 5. Dynamic response of the #1 inverter when the amplitude of v_g sees a 5% decrease. (a) U_{dc1}. (b) I_{a1}.

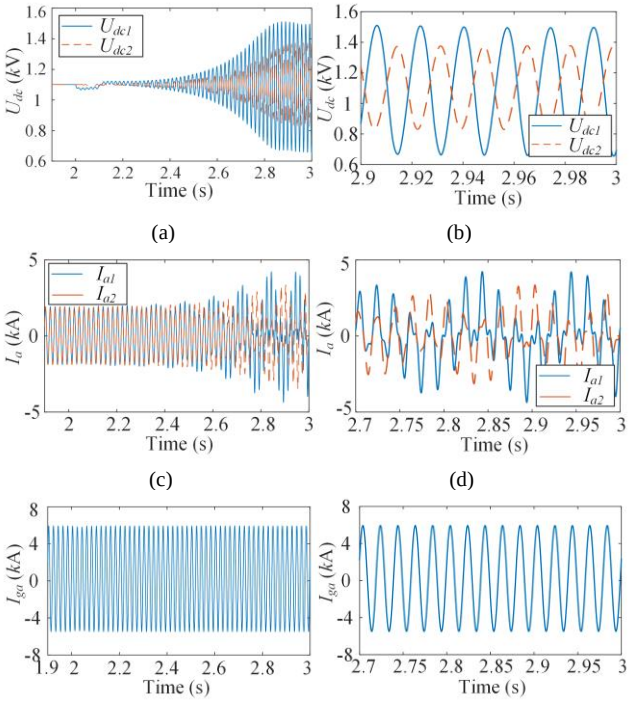

(a) (b)
(c) (d)
(e) (f)

Fig. 6. Dynamic responses of the #1 and #2 inverters when the P_{in} sees a 5% decrease. (a) U_{dc}. (b) Zoomed-in figure of U_{dc}. (c) I_a. (d) Zoomed-in figure of I_a. (e) I_{ga}. (f) Zoomed-in figure of I_{ga}.

in which $|\cdot|_1$ is the L_1-norm, the $\mathbf{p_{j,l}}$ is the vector with participation factors of all the state variables of #j inverter in mode l, and the $\mathbf{p_l}$ is the vector with participation factors of all the state variables of the whole system in mode l.

It has been stated in [19] that if $\eta_{al}>\varepsilon$ and $\eta_{bl}>\varepsilon$, where ε is a specified threshold, the mode l is an interaction mode in which state variables of #a inverter and #b inverter both dominantly participate.

A. Interaction Phenomena

When three inverters have identical dc input power, 1.5 MW each, the eigenvalues of the system are calculated based on the state-space model of paralleled inverters referring to [24] and [25]. Fig. 3 shows the eigenvalues. When the specified threshold ε is set as 0.1, only one mode is classified as a local mode, which is marked as orange crosses in Fig. 3. IMs exist in all time-scale dynamics. Because the three pairs of medium-frequency (50-200Hz) modes have low or even negative damping ratios for this 3-inverter system, the medium-frequency dynamics is studied in this paper. It can be seen from Fig. 3 that there are IMs on the right-half plane. The shape of the medium-frequency IMs and corresponding OPI η are listed in Table II. In Table II, the frequency and damping

ratio of modes 3, 4, 6 and 7 is identical, so they are overlapped in Fig. 3. The participation factor of all the state variables associated with medium-frequency IMs are shown in Fig. 4. Only I_{dref}, I_d, and γ_d participate in the medium-frequency IMs. The I_d and the γ_d, which is the derivative of I_d, are related with current control, while I_{dref} is related with dc voltage control. Thus, only parameters of the current control and the dc voltage control affect the dynamic characteristics of medium-frequency IMs. In addition, parameters of the current control play a leading role in medium-frequency IMs, because I_d and γ_d dominantly participate in these modes compared to I_{dref}.

No matter what perturbation is imposed on paralleled inverters connected to a weak grid, the dynamic response of each inverter is interacted with that of another. The reason is that the voltage at PCC can be changed by the total current of all the inverters, which can be affected by the current of any inverter. Meanwhile, the dynamic responses of any inverter can be influenced by PCC voltage. In this way, there are interactions among weak-grid-connected inverters under any perturbations. The interaction phenomena of the three-inverter system are observed under two kinds of perturbation by simulation of the detailed model of three inverters on PSCAD. One kind is a disturbance outside the cluster of inverters, which can make all the inverters experiencing identical perturbations, another is a disturbance inside the cluster, which generate the difference in perturbations on each inverter.

Firstly, the amplitude of v_g is decreased at 2.0 s. Because the v_g perturbation is outside the three identical inverters, the responses of three inverters are the same in this case. The dynamic responses of dc-link voltage U_{dc} and A-phase current I_a of #1 inverter are shown in Fig. 5. It is observable that the inverters are stable. **This result implies that the right-half-plane (RHP) mode is not excited by the perturbation on v_g.**

Secondly, the P_{in1} sees a 5% decrease at 2.0 s, while comes back to 1.5 MW at 2.1 s. The simulation results are shown in Fig. 6. In this case, the instability shows in the dynamic responses of each inverter after 2.0 s. However, the total current flowing into the grid is stable. **It indicates that the RHP IM can be excited by the perturbation on P_{in1}, but it cannot affect the total current or power output of a cluster of inverters.** It is worth mentioning that the currents and voltage shown in Fig. 6 do not diverge in this unstable case, because of the nonlinearity of pulse width modulation (PWM).

It can be seen from Fig. 5 and Fig. 6 that the perturbation outside a cluster of inverters and the perturbation inside the cluster can generate different interaction phenomena. Meanwhile, the difference in perturbations of each inverter can excite the RHP IMs of this 3-inverter system. Traditional single-inverter aggregation method, which aggregates identical or coherent inverters as a single up-scaled inverter model, cannot reveal the difference of inverters in perturbations, and thus is inapplicable to stability analysis of inverters in weak grids. The reasons for these interaction phenomena are theoretically analyzed by modal analysis in the next part.

B. Analysis on Interaction Characteristics

In this part, the concepts of controllability and observability are introduced to explain the interaction phenomena presented in section II-A. The controllability is used to explain the condition of modes excitation, and the observability is used to explain the reason why the RHP IMs cannot affect the grid current. The state-space model of a weak-grid-connected multi inverter system should be established before controllability and observability analyses.

This model can be established referring to [24] and [25]:

$$\Delta\dot{\mathbf{X}} = \mathbf{A}\Delta\mathbf{X}, \tag{2}$$

in which $\mathbf{X}$ is the state variable vector of multi-inverter systems, $\mathbf{X}=[\mathbf{X_1}^{\mathrm{T}}, \mathbf{X_2}^{\mathrm{T}}, ..., \mathbf{X_n}^{\mathrm{T}}]^{\mathrm{T}}$, n is the number of inverters paralleled, $\mathbf{X}_j=[U_{dcj}, I_{drefj}, I_{dj}, \gamma_{dj}, I_{qj}, \gamma_{qj}, \theta_j, \omega_j]^{\mathrm{T}}$ for inverters with VOC, and $\mathbf{A}=\begin{bmatrix} \mathbf{A_{11}} & \mathbf{A_{12}} & ... & \mathbf{A_{1n}} \\ \mathbf{A_{21}} & \mathbf{A_{22}} & ... & \mathbf{A_{2n}} \\ ... & ... & ... & ... \\ \mathbf{A_{n1}} & \mathbf{A_{n2}} & ... & \mathbf{A_{nn}} \end{bmatrix}$.

The detailed derivation of the state matrix $\mathbf{A}$ is presented in Appendix A.

The controllability and observability analyses are conducted based on specific input and output variables. Thus, the state-space model including the influence of input variables and the responses of output variables should be established as well:

$$\begin{cases} \Delta\dot{\mathbf{X}} = \mathbf{A}\Delta\mathbf{X} + \mathbf{B}\Delta\mathbf{U} \\ \Delta\mathbf{Y} = \mathbf{C}\Delta\mathbf{X} + \mathbf{D}\Delta\mathbf{U} \end{cases} \tag{3}$$

in which $\mathbf{U}=[U_1, U_2, \ldots, U_m]^{\mathrm{T}}$ is an m-order input vector, and $\mathbf{Y}=[Y_1, Y_2, \ldots, Y_s]^{\mathrm{T}}$ is an s-order output vector. U_m is the mth input variable in $\mathbf{U}$, and Y_s is the sth output variable in $\mathbf{Y}$. The detailed expressions of matrices $\mathbf{B}$, $\mathbf{C}$, and $\mathbf{D}$ depend on the composition of $\mathbf{U}$ and $\mathbf{Y}$.

The state-space model shown in (3) can be diagonalized as

$$\begin{cases} \Delta\dot{\mathbf{Z}} = \mathbf{\Lambda}\Delta\mathbf{Z} + \mathbf{u}^{-1}\mathbf{B}\Delta\mathbf{U} \\ \Delta\mathbf{Y} = \mathbf{C}\mathbf{u}\Delta\mathbf{Z} + \mathbf{D}\Delta\mathbf{U} \end{cases} \tag{4}$$

in which $\mathbf{\Lambda}=\mathrm{diag}(\lambda_1, \lambda_2, \ldots \lambda_{8n})$, $\mathbf{u}$ is the left eigenvalue vector, λ is an eigenvalue, and n is the number of inverters.

If elements of the row l of $\mathbf{u}^{-1}\mathbf{B}$ are all zeros, the corresponding state z_l cannot be controlled by any control variable in $\mathbf{U}$ [26]. The dynamic characteristics of each z_l is determined by the corresponding mode shape λ_l, because the $\mathbf{\Lambda}$ in (4) is a diagonal matrix. Thus, controllability of states z_l can also be equivalent to the controllability of λ_l. According to the definition of controllability [26], if a mode is controllable corresponding to a specific $\mathbf{U}$, this mode can be excited by this control vector $\mathbf{U}$.

Because $\mathbf{u}^{-1}=\mathbf{v}^{\mathrm{T}}$, the $\mathbf{u}^{-1}\mathbf{B}$ can be rewritten as

$$\mathrm{row}(\mathbf{u}^{-1}\mathbf{B}, l) = \sum_{j=1}^{n}(\mathbf{v}_{jl}^{\mathrm{T}}\mathbf{B}_j) \tag{5}$$

in which $\mathrm{row}(\mathbf{u}^{-1}\mathbf{B}, l)$ represents the row l of the matrix $\mathbf{u}^{-1}\mathbf{B}$, $\mathbf{v}_{jl}^{\mathrm{T}}=[v_{8j-7,l}, v_{8j-6,l}, \ldots v_{8j,l}]$, $\mathbf{B}_j$ is the submatrix of $\mathbf{B}$ from row $8j$-7 to row $8j$.

In this way, the controllability can be analyzed by identifying whether $\sum_{j=1}^{n}(\mathbf{v}_{jl}^{\mathrm{T}}\mathbf{B}_j)$ is 0.

When the perturbations on all the inverters are the same, we have $\mathbf{B_1}=\mathbf{B_2}=\ldots=\mathbf{B}_n$, and thus

$$\sum_{j=1}^{n}(\mathbf{v}_{jl}^{\mathrm{T}}\mathbf{B}_j) = \mathbf{B}_1\sum_{j=1}^{n}\mathbf{v}_{jl}^{\mathrm{T}} \tag{6}$$

This article has been accepted for publication in a future issue of this journal, but has not been fully edited. Content may change prior to final publication. Citation information: DOI 10.1109/JESTPE.2020.2988364, IEEE Journal of Emerging and Selected Topics in Power Electronics

It is obtained from the modal analysis of the three-inverter example system that when l equals to 3, 4, 6, or 7, which is the serial number (SN) of RHP medium-frequency IMs, the $\sum_{j=1}^{n}\mathbf{v}_{jl}^{\mathrm{T}}$ is a zero vector. However, when l equals to 1 or 2, which is the SN of left-half plane (LHP) IMs, the $\sum_{j=1}^{n}\mathbf{v}_{jl}^{\mathrm{T}}$ is nonzero. It indicates that the RHP IMs are uncontrollable and LHP IMs are controllable under a disturbance which can make all the inverters experiencing identical perturbations. It means that when perturbations on each inverter are identical, the RHP IMs of the three-inverter example system cannot be excited, while the LHP IMs can. This can explain the dynamic responses of the example system shown in Fig. 5.

When there is a difference in perturbations of inverters, (6) does not hold any more, and row ($\mathbf{u}^{-1}\mathbf{B}$, l) is a nonzero vector for l equaling to 3, 4, 6, or 7. In this way, RHP IMs can be excited. This can explain the unstable dynamic responses shown in Fig. 6 (a)-(d).

In addition, observability is used to analyze whether the transition of a state can affect the specific output vector. The observability of the mode λ_l is equivalent to the observability of the state z_l in a diagonalized system shown in (4).

If the elements of column l of **Cu** are all zeros, the corresponding z_l cannot be observed by any outputs in **Y** [26]. It means that mode l does not affect output **Y**. When the output is the sum of d-axis currents flowing to the grid, the column l of **Cu** is

$$\mathrm{col}(\mathbf{Cu}, l) = \sum_{j=1}^{n} u_{8(j-1)+3,l}\ , \tag{7}$$

in which col (**Cu**, l) is the column l of the matrix **Cu**.

It can be known from the modal analysis of the example system that if the output variable is set as the grid current, col(**Cu**, l) is a nonzero vector for l equaling to the SN of LHP IMs. However, for l equaling to the SN of RHP IMs, the col(**Cu**, l) is a zero vector. It indicates that the LHP IMs are observable and RHP IMs are unobservable by the grid current. This can explain the reason why grid current is stable, even though the RHP IMs are excited, as is shown in Fig. 6 (e) and (f).

From the above controllability and observability analyses, the IMs are classified into two types. In this paper, the controllable and observable IMs are called as Type-I IMs, and the uncontrollable and unobservable IMs are called as Type-II IMs. It is worth mentioning that the controllability and observability analyses in this paper are under the premise that **U** is the input variable vector which can make all the inverters experiencing identical perturbations and that the output variable vector **Y** is the grid current.

To further explore the physical meaning of Type-I and Type-II IMs, the common current components and interactive current components are defined respectively in (8) and (9).

$$I_{\mathrm{com}} = \frac{\sum_{j=1}^{n} I_j}{n} \tag{8}$$

$$I_{\mathrm{int}\,j} = I_j - I_{\mathrm{com}} \tag{9}$$

In (8), the I_{com} represents the common current components. In (9), the I_j is the current of #j inverter, and $I_{\mathrm{int}j}$ represents the interactive current components of #j inverter. For inverters with constant q-axis current reference shown in Fig. 2, only d-axis currents of paralleled inverters are interacted, and the I_j in (9) refers to d-axis current of #j inverter in particular.

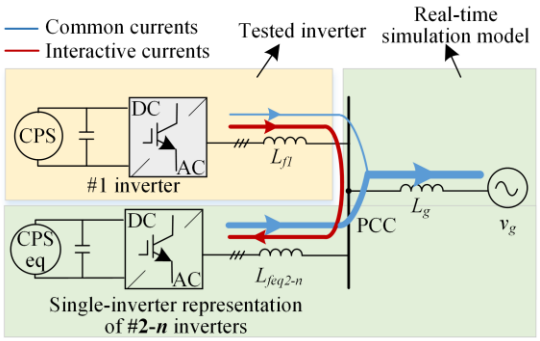

Fig. 7. Emulation of multi-inverter integrated weak grid based on two-inverter aggregation.

When perturbations on each inverter are identical, the inverters have identical current responses. In this way, the output current of every inverter in parallel purely consists of common current components. Thus, Type-I IMs, which are controllable by identical perturbations on inverters, affect the dynamic responses common current components of the system, and has no relation with the stability of interactive current components. By contrast, there are interactive current components among inverters when perturbations of inverters are different. Type-II IMs, which are only controllable by different perturbations on inverters, affect the stability of interactive current components, and does not affect the characteristics of common current components.

The example system is the simplest but a typical case of multiple inverters in parallel. The interaction characteristics can be extended to cases where more inverters are paralleled and also be extended to the interaction analyses in other time scales.

It is obvious that the external characteristics of a cluster of inverters, i.e., the characteristics of the total current flowing into the grid, is consistent with that of common current components. The external characteristics of a cluster of inverters can be preserved by traditional single-inverter aggregation [2], [3]. Thus, it can be applicable to the dynamic analysis of a study system outside inverters. However, the traditional single-inverter aggregation cannot preserve the characteristics of interactive current components, so it cannot completely describe the stability of multiple inverters connected to a weak grid.

III. Grid Emulation with Interaction-Preserved Aggregation

In this section, an emulation method for multi-inverter integrated weak grids is proposed to reveal stability problems affected by interaction among inverters. This emulation method is based on the two-inverter aggregation, which can preserve the dynamic characteristics of both common current components and interactive current components.

A. Grid Emulation Based on Two-Inverter Aggregation

As is analyzed in Section II-B, the stability of common current and interactive current components is independently

This article has been accepted for publication in a future issue of this journal, but has not been fully edited. Content may change prior to final publication. Citation information: DOI 10.1109/JESTPE.2020.2988364, IEEE Journal of Emerging and Selected Topics in Power Electronics

TABLE III
PARAMETERS OF THE TWO-INVERTER AGGREGATED MODEL

Symbols	S (MW)	L_f (mH)	C (10^3μF)	k_{pv}	k_{iv}	k_{ii}	k_{pt}	k_{it}
#1	1.5	0.2	11.75	3	20	20	50	900
Eq. #2	22.5	0.0133	176.25	45	300	1.33	50	900

TABLE IV
PARAMETERS OF THE SINGLE-INVERTER AGGREGATED MODEL

Symbols	S (MW)	L_f (mH)	C (10^3μF)	k_{pv}	k_{iv}	k_{ii}	k_{pt}	k_{it}
Eq.	24	0.0125	188	48	320	1.25	50	900

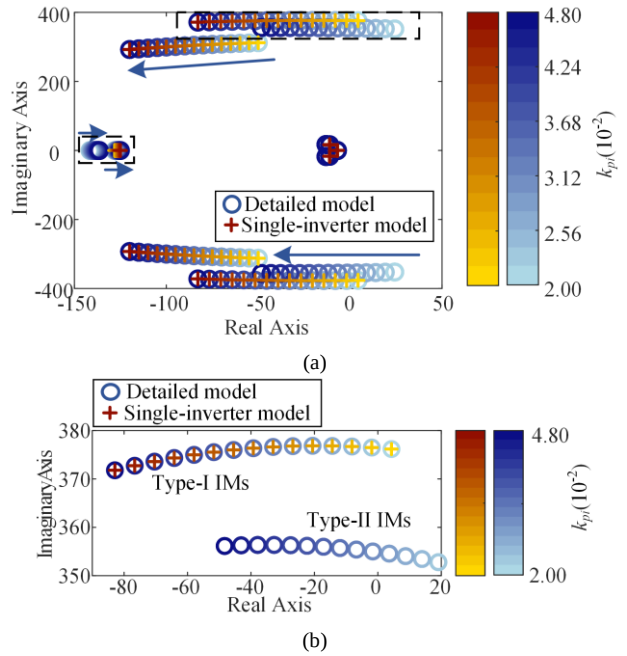

Fig. 8. Modes of the detailed model and single-inverter model corresponding to the variation in the proportional coefficient of current controller k_{pi}. (a) All modes of the two models. (b) Type-I and Type-II medium-frequency modes of the two models.

determined by Type-I IMs and Type-II IMs, respectively. Besides, the Type-II IMs can be excited in any cases where interactive currents exist. It is obvious that the dynamic responses of multiple paralleled inverters under a perturbation on any inverter can predict the instability phenomena of interactive currents. Assume that only #1 inverter is perturbed, the line currents of #2-*n* inverters are identical, and the interactive currents flow from 1# inverter to #2-*n* inverters. Thus, #2-*n* inverters can be aggregated as a single up-scaled inverter as shown in Fig. 7. One real inverter and one aggregated inverter model, which is called as two-inverter representation in this paper, can be used to analyze the stability of interactive currents. As is shown in Fig. 7, only one practical inverter needs to be tested, while #2 equivalent inverter and weak grid can be modeled and calculated in a real-time simulator. This emulation method can down-scale the testbed and simplify the test process for the parameter design of multiple weak-grid-tied inverters.

The equivalent parameters of the aggregated model of #2-*n* inverters are also calculated based on the aggregation algorithm for single-inverter aggregated models [4-6], [26]. The equivalent parameters are calculated to guarantee the correspondence between the power output of the aggregated model and the total power output of paralleled inverters. Thus, the parameters of the equivalent model of #2-*n* inverters are

$$L_{feq} = L_{fj} / (n-1)\,,\ C_{eq} = (n-1)C_j\,, \tag{10.1}$$

$$k_{pveq} = (n-1)k_{pvj}\,,\ k_{iveq} = (n-1)k_{ivj}\,, \tag{10.2}$$

$$k_{pieq} = k_{pij} / (n-1)\,, k_{iieq} = k_{iij} / (n-1)\,, \tag{10.3}$$

$$k_{pteq} = k_{ptj}\,,\ k_{iteq} = k_{itj}\,, \tag{10.4}$$

in which j can be any number between 2 and n.

The procedure of the application of the emulation method is presented as follows:

(i) calculating the equivalent parameters of n-1 inverters following the algorithm shown in equation (10);

(ii) establishing the aggregated model of #2-n inverters in a real-time simulator using the equivalent parameters calculated in step (i);

(iii) generating interactive currents between two inverters and testing their dynamic responses.

Stable dynamic responses of two inverters under perturbation on #1 inverter means that both common current components and interactive current components of the two inverters are stable. Then it can be inferred that every individual inverter in a real system is stable. Otherwise, the parameters should be tuned to achieve the stability of individual inverters. In this way, the instability phenomenon of individual inverters can be identified by a two-inverter model efficiently.

B. System Modal Analysis

Sixteen identical paralleled inverters connected to a weak grid (SCR=3) are set as a test system for the verification of the proposed two-inverter aggregation. The X/R ratio of the simulated system is 10, and the grid impedance Z_g is 0.0066 Ω. The configuration of multiple weak-grid-connected inverters is presented in Fig. 1. The parameters of every individual inverter, except for the proportional coefficient of current controller, are the same with what have been listed in Table I.

The parameters of the proposed two-inverter aggregated model are calculated based on (10), and are listed in Table III. In the two-inverter representation, the equivalent inverter model of n-1 actual inverters is represented by equivalent #2 inverter, and abbreviated as "Eq. #2" in Table III. The single-inverter aggregated model is also established for comparison, and its parameters are listed in Table IV.

The modes of the detailed model, single-inverter aggregated model, and two-inverter aggregated model are calculated based on the linearized state-space model. Because the medium-frequency IMs are associated with state variables of dc-voltage controller and d-axis current controller, the values of k_{pv}, k_{iv}, k_{pi}, and k_{ii} can affect the characteristics of medium-frequency IMs. In this section, the k_{pi} is changed as an example for the comparison of root loci of the detailed model, single-inverter aggregated model, and two-inverter aggregated model. The k_{pi} of each individual inverter is changed from 0.02 to 0.048. The root loci of the detailed model and the single-inverter aggregated model corresponding to the change of k_{pi} are shown in Fig. 8 (a), and Fig. 8 (b) shows the enlarged view of medium-frequency IMs. It can be seen from Fig. 8 that the decrease in the k_{pi} contributes to rightward shifts of medium-frequency modes, and thus adversely affects the stability of medium-frequency dynamics. Besides, it is obvious

This article has been accepted for publication in a future issue of this journal, but has not been fully edited. Content may change prior to final publication. Citation information: DOI 10.1109/JESTPE.2020.2988364, IEEE Journal of Emerging and Selected Topics in Power Electronics

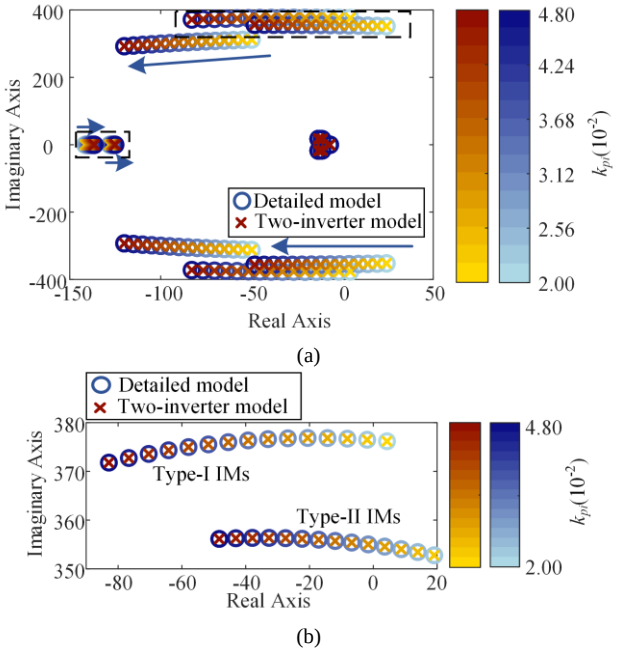

Fig. 9. Modes of the detailed model and the proposed two-inverter model corresponding to variation in the proportional coefficient of current controller k_{pi}. (a) All modes of two models. (b) Type-I and Type-II medium-frequency modes of two models.

from Fig. 8 that the dynamics of Type-II IMs of the detailed model cannot be represented by the single-inverter aggregated model. The reason is that the dynamic characteristics of interactive currents among inverters cannot be revealed by one inverter.

Fig. 9 compares the root loci of the detailed model and two-inverter representation model. The two-inverter aggregation can preserve both Type-I and Type-II IMs. In parallel, the variation trends of all modes of the proposed aggregated model corresponding to the increase in k_{pi} are the same with those of the detailed model. Therefore, the dynamic characteristics of interactive currents is preserved, and the stability issues of individual inverters in weak grids can be described by the proposed model in a simplified way.

To analyze the applicability of the proposed two-inverter model in grids with different strengths, the medium-frequency IMs of the detailed model, single-inverter aggregated model, and two-inverter aggregated model corresponding to the change in SCR from 3 to 15 are compared in Fig. 10. It can be seen in Fig. 10 that single-inverter model can only preserve the Type-I IMs, but cannot represent the dynamics of Type-II IMs of the detailed model connected to a grid with different strengths. However, the Type-II IMs of the detailed model can be preserved by the proposed two-inverter model in weak grids.

It is observable from Fig. 10 that when the SCR is smaller and the grid become weaker, the eigenvalues of the Type-I IMs and the Type-II IMs of the system are farther away from each other. The relative deviation of the damping ratio of Type-I and Type-II IMs with varied SCR is shown in Fig. 11. When the SCR is lower than 40, there is a big difference between the damping ratio of Type-I IMs and Type-II IMs, and thus the single-inverter model, which can only preserve the better-damped Type-I IMs, cannot comprehensively predict the stability arising from interactions. In these cases, the

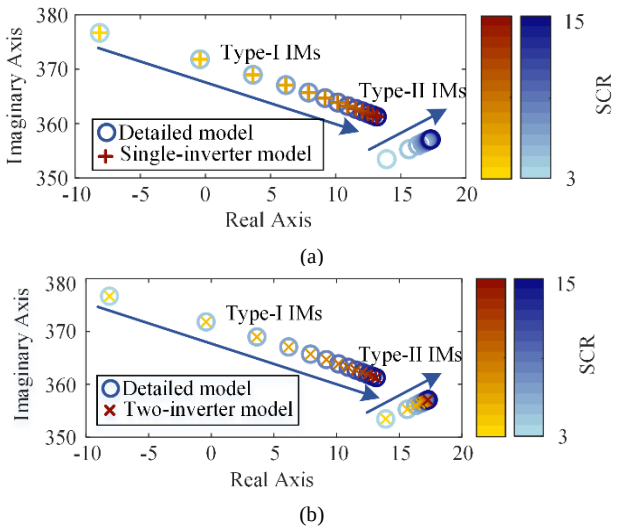

Fig. 10 Medium-frequency IMs of the detailed model, single-inverter aggregated model, and two-inverter aggregated model corresponding to the change in SCR from 3 to 15. (a) Medium-frequency IMs of the detailed model and single-inverter aggregated model. (b) Medium-frequency IMs of the detailed model and two-inverter aggregated model.

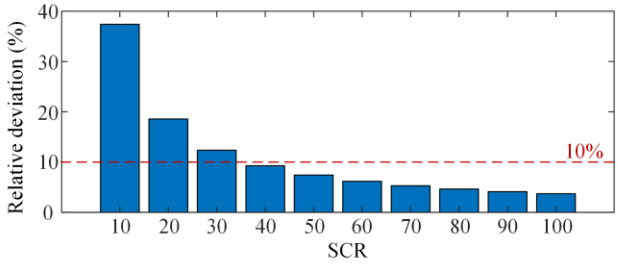

Fig. 11 The relative deviation of the damping ratio of Type-I and Type-II IMs of the 16-inverter-paralleled system when the SCR is changed from 10 to 100.

two-inverter model can show the advance in preserving the impact of interactions on stability.

When inverters with identical parameters are connected to an ideal grid, the Type-I and Type-II IMs are overlapped, and the dynamic characteristics of common currents and interactive currents is the same. In this case, the single-inverter aggregated model, which can preserve the dynamics of common currents, is adequate for describing the stability of paralleled inverters. Therefore, it is worth mentioning that the two-inverter aggregated model can show its advantage only when inverters are connected to a weak grid.

IV. Simulation and Controller Hardware-in-the-Loop Test Bench

A. *Simulation Verification of Two-Inverter Aggregation*

The detailed model, single-inverter aggregated model, and two-inverter aggregated model of the sixteen-inverter system in Section III are built in PSCAD/EMTDC. An unstable case when k_{pi}=0.023 and a stable case when k_{pi}=0.03 are simulated. Because the medium-frequency modes are close to the imaginary axis or even on the right-half plane, the medium-frequency dynamics of the detailed model and two aggregated models is discussed in this paper.

This article has been accepted for publication in a future issue of this journal, but has not been fully edited. Content may change prior to final publication. Citation information: DOI 10.1109/JESTPE.2020.2988364, IEEE Journal of Emerging and Selected Topics in Power Electronics

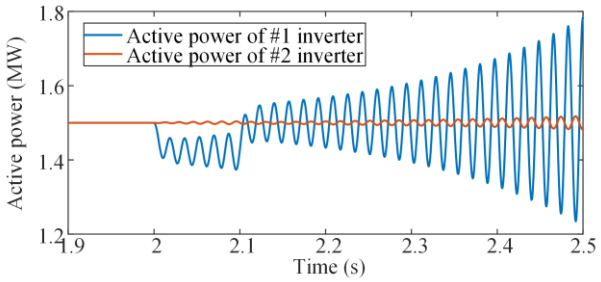

Fig. 12. Active power responses of #1 and #2 inverters of the detailed model in the unstable case (k_{pi}=0.023).

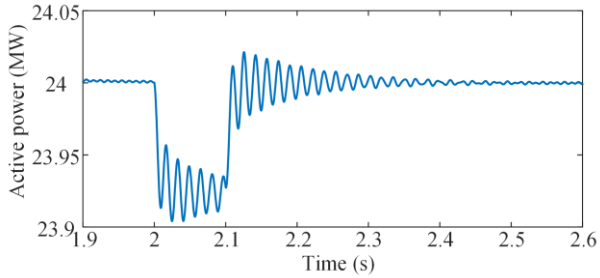

Fig. 13. Active power response of the single-inverter aggregated model under the perturbation at 2.0 s.

1) Case I: Unstable Case with k_{pi}=0.023

When k_{pi} of each inverter is 0.023, it can be seen from Fig. 9 that the medium-frequency Type-I IMs are on the left-half plane, while the medium-frequency Type-II IMs are on the right-half plane. It means that the common currents are stable, but the interactive currents are unstable. The instability of interactive currents is verified by simulation.

The 5% decrease, i.e., 0.075 MW decrease, in power input of #1 inverter at 2.0 s is used to excite interactive currents among inverters. The decrease in power input lasts 0.1 s. The same perturbation is imposed on #1 inverter of the two-inverter model, as well as the power input of the single-inverter model. The dynamic responses of three different models are shown in Fig. 12-14.

Fig. 12 shows the simulation results of the detailed model. The active power output of #1 inverter is shown by the blue solid line in Fig. 12. The output active power of #2-16 inverters is identical, so only that of #2 inverter is shown by the orange solid line in Fig. 12. As the simulation results of the detailed model shows, the unstable Type-II IM is excited by the perturbation.

The active power output of the single-inverter model is shown in Fig. 13. It is obvious in Fig. 13 that the single-inverter model is stable, which agrees with the modal analysis result. The stability analysis result of this model is opposite from that of the detailed model, because only the dynamic characteristics of common currents is preserved in this single-inverter model. The dynamic characteristics of interactive current components cannot be described in a single-inverter model.

The simulation results of the proposed two-inverter representation model are shown in Fig. 14. No perturbation is imposed on the two-inverter model, and the instability of the two inverters still shows in this case. It is because the capacity of #1 inverter and equivalent #2 inverter is different and there is interactive current between these two inverters when they are connected to the grid.

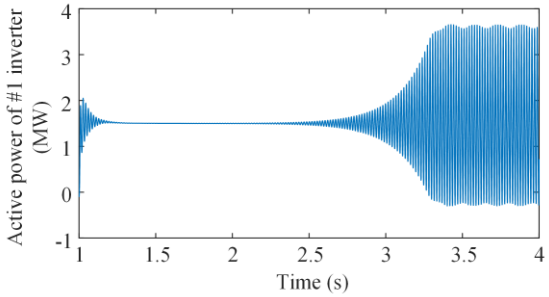

(a)

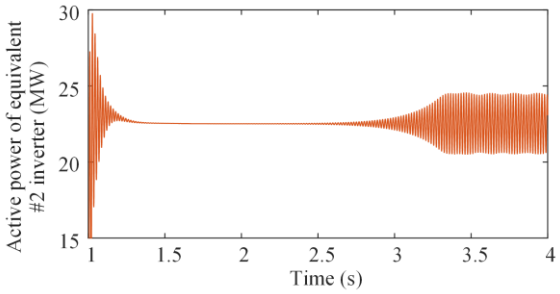

(b)

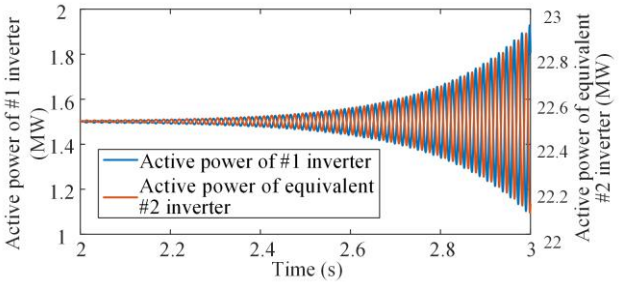

(c)

Fig. 14. Active power output of #1 and equivalent #2 inverters of the proposed two-inverter model. (a) Active power output of #1 inverter. (b) Active power output of equivalent #2 inverter. (c) Zoomed-in comparison in power output of #1 and equivalent #2 inverter.

From the analysis above, it is obvious that the stability of the proposed aggregated model corresponds to that of the detailed model. Therefore, the dynamic response of the two-inverter model can predict the stability of multiple inverters, though the interactions affect the stability of individual ones.

2) Case II: Stable Case with k_{pi}=0.03

When k_{pi} of each inverter in the example system is 0.03, it can be seen from Fig. 9 that all the modes are on the left-half plane. It means that both common current and interactive current are stable. The perturbations imposed on the detailed model and the single-inverter model are the same as those in case I. The dynamic responses of three models are presented in Fig. 15.

The comparison in results shown in Figs. 15 (a) and 15 (b) indicates that the settling time of the single-inverter model is shorter than that of the detailed model. The damping of the system cannot be accurately described by the single-inverter model. It is because the Type-II IMs are worse damped than Type-I IMs, but the Type-II IMs cannot be preserved by the single-inverter model. By contrast, the active power output of #1 inverter obtained by the proposed two-inverter model can fit the practical power curve in the detailed model. Besides, the active power of equivalent #2 inverter shown by the orange line

This article has been accepted for publication in a future issue of this journal, but has not been fully edited. Content may change prior to final publication. Citation information: DOI 10.1109/JESTPE.2020.2988364, IEEE Journal of Emerging and Selected Topics in Power Electronics

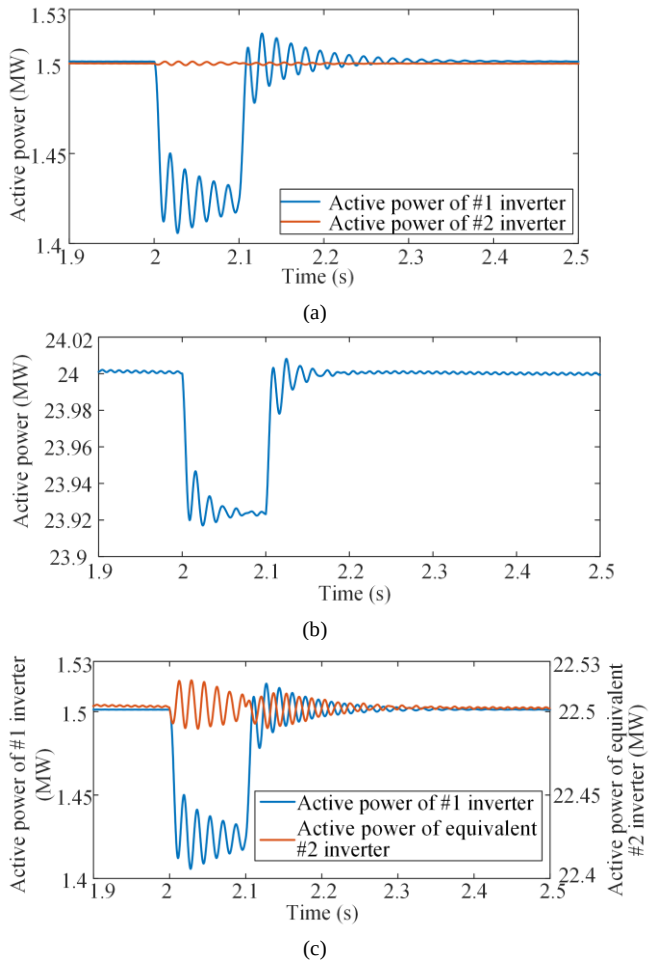

Fig. 15. Active power of three different models in the stable case (k_{pi}=0.03). (a) Active power output of #1 and #2 inverters of the detailed model. (b) Active power output of the single-inverter model. (c) Active power output of #1 and equivalent #2 inverters of the proposed two-inverter model.

in Fig. 15 (c), is 15 times of that of #2 inverter in the detailed model shown in Fig. 15 (a).

Both case I and case II validate that the two-inverter model can preserve the interaction of multiple inverters and then help identify the stability issues of individual inverters caused by interactions in a simplified way.

B. Controller Hardware-in-the-Loop Test Bench

The emulation of the 16-inverter example system is implemented on a controller HIL test bench. The instability shown in case I is validated by the HIL test. Fig. 16 shows the configuration of the testbed, which includes the real-time simulator (OPAL-RT OP5600) and the control board STM32F417ZET6. The #1 inverter is controlled by the control board, and the equivalent #2 inverter together with the weak grid impedance are simulated in OP5600. The parameters of #1 inverter and equivalent #2 inverter are the same with those in Table III.

The experimental results are shown in Fig. 17. Three-phase currents and dc-bus voltage of #1 inverter are recorded. It can be seen from Fig. 17 that #1 inverter is unstable, which corresponds to the simulation results. The instability attributing to interactions is identified by the HIL testbed. This

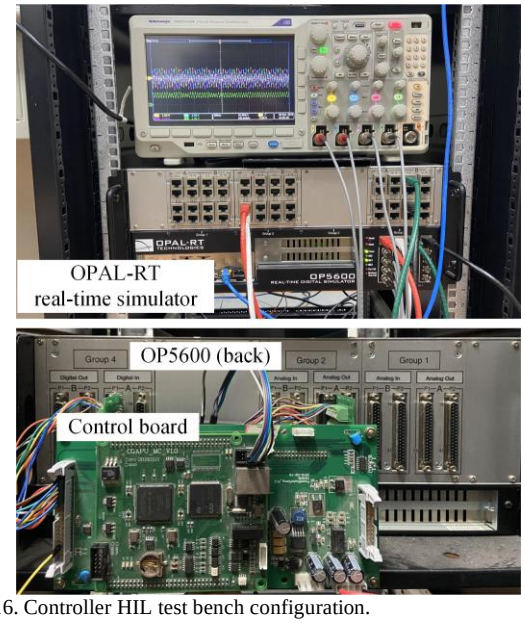

Fig. 16. Controller HIL test bench configuration.

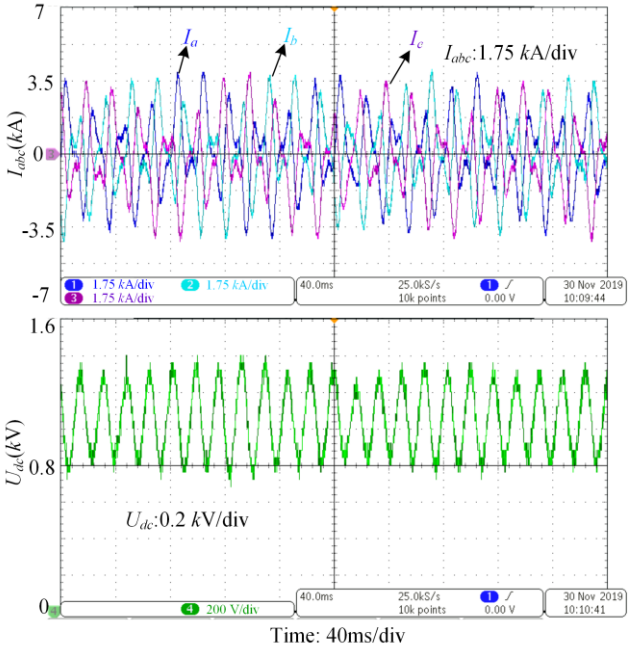

Fig. 17. HIL experiment results: three-phase currents I_{abc} and dc-link voltage U_{dc} of #1 inverter.

implementation also verifies the feasibility of testing the stability of multi-inverter systems using the simple two-inverter representation.

V. Conclusion

This paper proposes a novel emulation method of multi-inverter integrated weak grids using the two-inverter aggregation. The interaction characteristics of paralleled inverters with identical parameters is analyzed by controllability and observability analyses of multiple inverters, and then the two-inverter representation is developed based on the feature of interactions that the stability of interactive currents can be excited whenever initial states or perturbations of every individual inverter are not completely the same.

Compared with the traditional single-inverter aggregated model, the proposed two-inverter aggregation can further identify the stability of interactive currents effectively and efficiently. Therefore, the test bench of multiple inverters with identical parameters can be simplified as one practical inverter under test associated with an aggregated model calculated in a real-time simulator.

The 16 inverters with 1.5 MW capacity each are set as an example for validation. Both simulation and HIL tests verify the effectiveness and advantages of the proposed two-inverter aggregation and emulation method for the stability analysis of paralleled identical inverters in weak grids. A basic case where inverters have identical parameters is studied in this paper. When there is a big difference in the dynamic characteristics of paralleled inverters attributed to the parameters difference, more inverters are needed to represent a multi-inverter system in tests. This will be further studied in our future work.

APPENDIX A

The general state-space modeling is adopted in our work for a single VOC-controlled inverter, as described in [24] and [25]. The model can be briefly represented as

$$s\Delta\mathbf{X}_j = \mathbf{A}_{pj}\Delta\mathbf{X}_j + \mathbf{B}_{pj}\Delta\mathbf{v}_{pdqj}, \quad (A.1)$$

where $\mathbf{v}_{pdqj}=[v_{pdj}, v_{pqj}]^T$, and the *d-q* frame for each inverter is the rotating frame which rotates at the output frequency of the PLL of this inverter. In (A.1), $\mathbf{A}_{pj}$ and $\mathbf{B}_{pj}$ are coefficient matrices, and $\mathbf{X}_j$ is the state variables vector of #*j* grid-connected inverter. Specifically, $\mathbf{X}_j=[U_{dcj}, i_{drefj}, i_{dj}, \gamma_{dj}, i_{qj}, \gamma_{qj}, \theta_j, \omega_j]^T$.

The dynamics of the equivalent inductor of the weak grid needs to be included in the model:

$$L_g d\sum_{j=1}^{n} i_{xyj}/dt + j\omega_0 L_g \sum_{j=1}^{n} i_{xyj} + R_g \sum_{j=1}^{n} i_{xyj} = v_{pxy} - v_{gxy} \quad (A.2)$$

in which n is the number of inverters paralleled, $i_{xyj}=i_{xj}+ji_{yj}$, $v_{pxy}=v_{px}+jv_{py}$, $v_{gxy}=v_{gx}+jv_{gy}$. The *x-y* frame is a synchronous rotating frame, and the *x* axis is oriented to the in finite bus voltage vector v_g.

When perturbations on v_g are not considered, equation (A.2) can be linearized as:

$$\Delta v_{pxy} = L_g d\sum_{j=1}^{n}\Delta i_{xyj}/dt + j\omega_0 L_g \sum_{j=1}^{n}\Delta i_{xyj} + R_g\sum_{j=1}^{n}\Delta i_{xyj}. \quad (A.3)$$

Because the i_{dj} and i_{qj} have been chosen as state variables as mentioned before, the components in *x-y* frame should be expressed by components in *d-q* frames for the state-space modeling:

$$\begin{bmatrix} i_{xj} \\ i_{yj} \end{bmatrix} = \begin{bmatrix} \cos\theta_j & -\sin\theta_j \\ \sin\theta_j & \cos\theta_j \end{bmatrix} \begin{bmatrix} i_{dj} \\ i_{qj} \end{bmatrix}. \quad (A.4)$$

The (A.4) can be linearized as:

$$\Delta\mathbf{i}_{xyj} = \mathbf{T}_j\Delta\mathbf{i}_{dqj} + \mathbf{K}_j\Delta\theta_j \quad (A.5)$$

where $\mathbf{T}_j = \begin{bmatrix} \cos\theta_{j0} & -\sin\theta_{j0} \\ \sin\theta_{j0} & \cos\theta_{j0} \end{bmatrix}$, $\mathbf{K}_j = \begin{bmatrix} -\sin\theta_{j0}i_{dj0} - \cos\theta_{j0}i_{qj0} \\ \cos\theta_{j0}i_{dj0} - \sin\theta_{j0}i_{qj0} \end{bmatrix}$, $\mathbf{i}_{xyj}=[i_{xj}, i_{yj}]^T$, and $\mathbf{i}_{dqj}=[i_{dj}, i_{qj}]^T$.

Similarly, there is

$$\Delta\mathbf{v}_{pxy} = \mathbf{T}_j\Delta\mathbf{v}_{pdqj} + \mathbf{K}_j\Delta\theta_j, \quad (A.6)$$

in which $\mathbf{v}_{pxy}=[v_{px}, v_{py}]^T$, and $\mathbf{v}_{pdqj}=[v_{pdj}, v_{pqj}]^T$.

By substituting (A.5) and (A.6) into (A.3), the relationship between $\Delta\mathbf{v}_{pdqj}$ and state variables vector can be obtained:

$$\Delta\mathbf{v}_{pdqj} = \mathbf{f}(\Delta i_{dm}, \Delta i_{qm}, \Delta\gamma_{dm}, \Delta\gamma_{qm}, \Delta\omega_m, \Delta\theta_m), \quad (A.7)$$

in which the subscript m=1, 2, ..., n.

Substituting (A.7) into (A.1) and combining the state equations of all the inverters, there is the state-space model of n paralleled inverters:

$$\Delta\dot{\mathbf{X}} = \mathbf{A}\Delta\mathbf{X}. \quad (A.8)$$

where $\mathbf{A} = \begin{bmatrix} \mathbf{A}_{11} & \mathbf{A}_{12} & \dots & \mathbf{A}_{1n} \\ \mathbf{A}_{21} & \mathbf{A}_{22} & \dots & \mathbf{A}_{2n} \\ \dots & \dots & \dots & \dots \\ \mathbf{A}_{n1} & \mathbf{A}_{n2} & \dots & \mathbf{A}_{nn} \end{bmatrix}$, and $\mathbf{X}=[\mathbf{X}_1^T, \mathbf{X}_2^T, ..., \mathbf{X}_n^T]^T$.

When n identical inverters are paralleled, the diagonal submatrices equal to each other, as well as the nondiagonal submatrices. The explicit expressions of the diagonal submatrix $\mathbf{A}_{ii}$ and nondiagonal matrix $\mathbf{A}_{ij}$ ($i\neq j$) are represented by

$$\mathbf{A}_{ii} = \begin{bmatrix} \mathbf{A}_{pii} \\ \mathbf{A}_{\theta ii} \\ \mathbf{A}_{\omega ii} \end{bmatrix}, \mathbf{A}_{ij} = \begin{bmatrix} \mathbf{A}_{pij} \\ \mathbf{A}_{\theta ij} \\ \mathbf{A}_{\omega ij} \end{bmatrix}, \quad (A.9)$$

in which $i, j \in \mathrm{N}$, and $i, j \in [1, n]$.

The matrices $\mathbf{A}_{pii}$, $\mathbf{A}_{pij}$, $\mathbf{A}_{\theta ii}$, $\mathbf{A}_{\theta ij}$, $\mathbf{A}_{\omega ii}$, and $\mathbf{A}_{\omega ij}$ are calculated by

$$\begin{cases} \mathbf{A}_{pii} = \mathbf{M}_i + \mathbf{N}_i\mathbf{T}_{ii} \\ \mathbf{A}_{pij} = \mathbf{N}_i\mathbf{T}_{ij} \\ \mathbf{A}_{\theta ii} = [0 \quad 0 \quad 0 \quad 0 \quad 0 \quad 0 \quad 0 \quad 1] \\ \mathbf{A}_{\theta ij} = [0 \quad 0 \quad 0 \quad 0 \quad 0 \quad 0 \quad 0 \quad 0] \\ \mathbf{A}_{\omega ii} = \mathbf{C}_i + \mathbf{D}_{ii} + \dfrac{k_{pt,i}L_g}{h}(i_{d0,i}\mathbf{C}_i + \sum_{m=1}^{n} i_{d0,m}\mathbf{D}_{mi}) \\ \mathbf{A}_{\omega ij} = \mathbf{D}_{ij} + \dfrac{k_{pt,i}L_g}{h}(i_{d0,j}\mathbf{C}_j + \sum_{m=1}^{n} i_{d0,m}\mathbf{D}_{mj}) \end{cases} \quad (A.10)$$

The expressions of $\mathbf{M}_i$, $\mathbf{N}_i$, $\mathbf{T}_{ij}$, h, $\mathbf{C}_i$, and $\mathbf{D}_{ij}$ are shown in (A.11)-(A.16).

$$h = 1 - L_g\sum_{i=i}^{n} i_{d0,i}k_{pt,i} \quad (A.14)$$

$$\mathbf{C}_i = \begin{bmatrix} 0 & 0 & 0 & 0 & 0 & 0 & -k_{it,i}v_{pd0,i} & -k_{pt,i}v_{pd0,i} \end{bmatrix} \quad (A.15)$$

In (A.13) and (A.16), the $m_{lk,i}$ represents the lth row and kth column of the matrix $\mathbf{M}_i$.

REFERENCES

[1] J. H. R. Enslin and P. J. M. Heskes, "Harmonic interaction between a large number of distributed power inverters and the distribution network," *IEEE Trans. Power Electron.*, vol. 19, no. 6, pp. 1586-1593, Nov. 2004.

[2] A. Adib, F. Fateh, M. B. Shadmand, and B. Mirafzal, "Weak grid impacts on stability of voltage source inverters -asymmetrical grid," in *2018 IEEE Energy Conversion Congress and Exposition (ECCE)*, Portland, OR, 2018, pp. 3055-3060.

This article has been accepted for publication in a future issue of this journal, but has not been fully edited. Content may change prior to final publication. Citation information: DOI 10.1109/JESTPE.2020.2988364, IEEE Journal of Emerging and Selected Topics in Power Electronics

$$\mathbf{M}_i = \begin{bmatrix} 0 & 0 & \frac{-3V_{pd0,i}}{2C_iU_{dc0,i}} & 0 & 0 & 0 & 0 & 0 \\ k_{iv,i} & 0 & -\frac{3k_{pv,i}V_{pd0,i}}{2C_iU_{dc0,i}} & 0 & 0 & 0 & 0 & 0 \\ 0 & 0 & 0 & \frac{1}{L_{f,i}} & 0 & 0 & 0 & 0 \\ k_{pi,i}k_{iv,i} & k_{ii,i} & -(\frac{3k_{pi,i}k_{pv,i}V_{pd0,i}}{2CU_{dc0,i}}+k_{ii,i}) & -\frac{k_{pi,i}}{L_{f,i}} & 0 & 0 & 0 & 0 \\ 0 & 0 & 0 & 0 & 0 & \frac{1}{L_{f,i}} & 0 & 0 \\ 0 & 0 & 0 & 0 & -k_{ii,i} & -\frac{k_{pi,i}}{L_{f,i}} & 0 & 0 \end{bmatrix} \tag{A.11}$$

$$\mathbf{N}_i = \begin{bmatrix} -\frac{3I_{d0,i}}{2C_iU_{dc0,i}} & -\frac{3k_{pv,i}I_{d0,i}}{2C_iU_{dc0.i}} & 0 & -\frac{3k_{pi,i}k_{pv,i}I_{d0,i}}{2C_iU_{dc0.i}} & 0 & 0 \end{bmatrix}^{\mathrm{T}} \tag{A.12}$$

$$\mathbf{T}_{ij} = \begin{bmatrix} 0 & 0 & R_g & L_g m_{34,j} & -\omega_0 L_g & 0 & -(\omega_0 L_g i_{d0,j} + R_g i_{q0,j}) & -L_g i_{q0,j} \end{bmatrix} \tag{A.13}$$

$$\mathbf{D}_{ij} = \begin{bmatrix} 0 \\ 0 \\ k_{it,i}\omega_0 L_g \\ k_{pt,i}\omega_0 L_g m_{34,j} \\ k_{pt,i}L_g m_{56,j}m_{65,j} + k_{it,i}R_g \\ k_{pt,i}L_g m_{56,j}m_{66,j} + k_{it,i}L_g m_{56,j} + k_{pt,i}R_g m_{56,j} \\ -k_{it,i}(\omega_0 L_g i_{q0,j} + R_g i_{d0,j}) \\ k_{it,i}L_g i_{d0,j} - k_{pt,i}\omega_0 L_g i_{q0,j} + k_{pt,i}R_g i_{d0,j} \end{bmatrix}^{\mathrm{T}} \tag{A.16}$$

[3] Z. Shuai, Y. Li, W. Wu, C. Tu, A. Luo and Z. J. Shen, "Divided DQ small-signal model: a new perspective for the stability analysis of three-phase grid-tied inverters," *IEEE Trans. Ind. Electron.*, vol. 66, no. 8, pp. 6493-6504, Aug. 2019.

[4] L. Jia, X. Ruan, W. Zhao, Z. Lin and X. Wang, "An adaptive active damper for improving the stability of grid-connected inverters under weak grid," *IEEE Trans. Power Electron.*, vol. 33, no. 11, pp. 9561-9574, Nov. 2018.

[5] Y. Ma, L. Yang, J. Wang, F. Wang and L. M. Tolbert, "Emulating full-converter wind turbine by a single converter in a multiple converter based emulation system," *2014 IEEE Applied Power Electronics Conference and Exposition - APEC 2014*, Fort Worth, TX, 2014, pp. 3042-3047.

[6] J. Brochu, C. Larose and R. Gagnon, "Validation of single- and multiple-machine equivalents for modeling wind power plants," *IEEE Trans. Energy Convers.*, vol. 26, no. 2, pp. 532-541, June 2011.

[7] V. Purba, S. V. Dhople, S. Jafarpour, F. Bullo and B. B. Johnson, "Reduced-order structure-preserving model for parallel-connected three-phase grid-tied inverters," in *IEEE Workshop Control Modeling Power Electron.*, Stanford, CA, 2017, pp. 1-7.

[8] Z. Shuai, Y. Peng, X. Liu, Z. Li, J. M. Guerrero and Z. J. Shen, "Dynamic equivalent modeling for multi-microgrid based on structure preservation method," *IEEE Trans. Smart Grid*, vol. 10, no. 4, pp. 3929-3942, July 2019.

[9] X. Zha, S. Liao, M. Huang, Z. Yang and J. Sun, "Dynamic aggregation modeling of grid-connected inverters using Hamilton's-action-based coherent equivalence," *IEEE Trans. Ind. Electron.*, vol. 66, no. 8, pp. 6437-6448, Aug. 2019.

[10] C. Li, J. Xu and C. Zhao, "A coherency-based equivalence method for MMC inverters using virtual synchronous generator control," *IEEE Trans. Power Del.*, vol. 31, no. 3, pp. 1369-1378, June 2016.

[11] P. J. Hart, R. H. Lasseter and T. M. Jahns, "Coherency identification and aggregation in grid-forming droop-controlled inverter networks," *IEEE Trans. Ind. Appl.*, vol. 55, no. 3, pp. 2219-2231, May-June 2019.

[12] S. Liao, X. Zha, X. Li, M. Huang, J. Sun, J. Pan and J. M. Guerrero, "A novel dynamic aggregation modeling method of grid-connected inverters: application in small-signal analysis," *IEEE Trans. Sustain. Energy*, vol. 10, no. 3, pp. 1554-1564, July 2019.

[13] J. L. Agorreta, M. Borrega, J. López and L. Marroyo, "Modeling and control of *N*-paralleled grid-connected inverters with LCL filter coupled due to grid impedance in PV plants," *IEEE Trans. Power Electron.*, vol. 26, no. 3, pp. 770-785, March 2011.

[14] F. Cavazzana, T. Caldognetto, P. Mattavelli, M. Corradin and I. Toigo, "Analysis of current control interaction of multiple parallel grid-connected inverters," *IEEE Trans. Sustain. Energy*, vol. 9, no. 4, pp. 1740-1749, Oct. 2018.

[15] M. Lu, X. Wang, P. C. Loh and F. Blaabjerg, "Resonance interaction of multiparallel grid-connected inverters with LCL filter," *IEEE Trans. Power Electron.*, vol. 32, no. 2, pp. 894-899, Feb. 2017.

[16] M. Lu, Y. Yang, B. Johnson and F. Blaabjerg, "An interaction-admittance model for multi-inverter grid-connected systems," *IEEE Trans. Power Electron.*, vol. 34, no. 8, pp. 7542-7557, Aug. 2019.

[17] L. Hong, W. Shu, J. Wang and R. Mian, "Harmonic resonance investigation of a multi-inverter grid-connected system using resonance modal analysis," *IEEE Trans. Power Del.*, vol. 34, no. 1, pp. 63-72, Feb. 2019.

[18] J. He, Y. W. Li, D. Bosnjak and B. Harris, "Investigation and active damping of multiple resonances in a parallel-inverter-based microgrid," *IEEE Trans. Power Electron.*, vol. 28, no. 1, pp. 234-246, Jan. 2013.

[19] J. Beerten, S. D'Arco and J. A. Suul, "Identification and small-signal analysis of interaction modes in VSC MTDC systems," *IEEE Trans. Power Del.*, vol. 31, no. 2, pp. 888-897, April 2016.
[20] Y. Wang, X. Wang, Z. Chen and F. Blaabjerg, "Small-signal stability analysis of inverter-fed power systems using component connection method," *IEEE Trans. Smart Grid*, vol. 9, no. 5, pp. 5301-5310, Sept. 2018.
[21] P. Hou, E. Ebrahimzadeh, X. Wang, F. Blaabjerg, J. Fang and Y. Wang, "Harmonic stability analysis of offshore wind farm with component connection method," *IECON 2017 - 43rd Annual Conference of the IEEE Industrial Electronics Society*, Beijing, 2017, pp. 4926-4932.
[22] R. Dimitrovski, A. Dolderer, G. Mehlmann, M. Luther, M. Ndreko and W. Winter, "Analyzing subsynchronous resonance using component connection method," *2018 IEEE Power & Energy Society General Meeting (PESGM)*, Portland, OR, 2018, pp. 1-5.
[23] S. Golestan and J. M. Guerrero, "Conventional synchronous reference frame phase-locked loop is an adaptive complex filter," *IEEE Trans. Ind. Electron.*, vol. 62, no. 3, pp. 1679-1682, March 2015.
[24] Y. Huang, X. Yuan, J. Hu and P. Zhou, "Modeling of VSC connected to weak grid for stability analysis of DC-link voltage control," *IEEE J. Emerg., Sel. Topics Power Electron.*, vol. 3, no. 4, pp. 1193-1204, Dec. 2015.
[25] W. Du, X. Chen and H. F. Wang, "Power system electromechanical oscillation modes as affected by dynamic interactions from grid-connected PMSGs for wind power generation," *IEEE Trans. Sustain. Energy*, vol. 8, no. 3, pp. 1301-1312, July 2017.
[26] K. Ogata, "Control systems analysis in state space," in Modern Control Engineering, fifth ed., Upper Saddle River, N. J., USA: Prentice Hall, 2009, 675-684.

Shuhan Liao (S'18) was born in Xiangtan, Hunan Province, China, in 1993. She received B. Eng. Degree in electrical engineering from Wuhan University, Wuhan, China, in 2015, where she is currently working toward the Ph. D. degree.
From Oct. 2018 to Oct. 2019, she was a guest Ph. D. student with the Department of Energy Technology, Aalborg University, Aalborg, Denmark. Her main research interests include the modeling and dynamic analysis of renewable energy generation systems.

Meng Huang (S'11–M'13) received the B.Eng. and M.Eng. degrees from Huazhong University of Science and Technology, Wuhan, China, in 2006 and 2008, respectively, and the Ph.D. degree from the Hong Kong Polytechnic University, Hong Kong, in 2013.
He is currently an Associate Professor of the School of Electrical Engineering and Automation, Wuhan University, Wuhan, China. His research interests include nonlinear analysis of power converters and power electronics reliability.

Xiaoming Zha (M'02) was born in Huaining, Anhui Province, China, in 1967. He received B.S., M.S., and Ph.D. degrees in electrical engineering from Wuhan University, Wuhan, China, in 1989, 1992, and 2001, respectively.
He was a Postdoctoral Fellow at the University of Alberta, Canada from 2001 to 2003. He has been a Faculty Member of Wuhan University since 1992, and became a Professor in 2003. He is currently the Deputy Dean in the school of Electrical Engineering and Automation, Wuhan University, Wuhan, China. His research interests include power electronic converter, the application of power electronics in smart grid and renewable energy generation, the analysis and control of microgrid, the analysis and control of power quality, and frequency control of high-voltage high-power electric motors.

Josep M. Guerrero (S'01-M'04-SM'08-FM'15) received the B.S. degree in telecommunications engineering, the M.S. degree in electronics engineering, and the Ph.D. degree in power electronics from the Technical University of Catalonia, Barcelona, in 1997, 2000 and 2003, respectively. Since 2011, he has been a Full Professor with the Department of Energy Technology, Aalborg University, Denmark, where he is responsible for the Microgrid Research Program (www.microgrids.et.aau.dk). From 2014 he is chair Professor in Shandong University; from 2015 he is a distinguished guest Professor in Hunan University; and from 2016 he is a visiting professor fellow at Aston University, UK, and a guest Professor at the Nanjing University of Posts and Telecommunications. From 2019, he became a Villum Investigator by The Villum Foundation, which supports the Centre for Research on Microgrids (CROM) at Aalborg University, being Prof. Guerrero the founder and Director of the same centre.
His research interests are oriented to different microgrid aspects, including power electronics, distributed energy-storage systems, hierarchical and cooperative control, energy management systems, smart metering and the internet of things for AC/DC microgrid clusters and islanded minigrids. Specially focused on maritime microgrids for electrical ships, vessels, ferries and seaports. Prof. Guerrero is an Associate Editor for a number of IEEE TRANSACTIONS. He has published more than 500 journal papers in the fields of microgrids and renewable energy systems, which are cited more than 30,000 times. He received the best paper award of the IEEE Transactions on Energy Conversion for the period 2014-2015, and the best paper prize of IEEE-PES in 2015. As well, he received the best paper award of the Journal of Power Electronics in 2016. During five consecutive years, from 2014 to 2018, he was awarded by Clarivate Analytics (former Thomson Reuters) as Highly Cited Researcher. In 2015 he was elevated as IEEE Fellow for his contributions on "distributed power systems and microgrids."